Materials Today Bio 25 (2024) 100967

Contents lists available at ScienceDirect

Materials Today Bio

journal homepage: www.journals.elsevier.com/materials-today-bio

Injectable thermosensitive selenium-containing hydrogel as mesenchymal stem cell carrier to improve treatment efficiency in limb ischemia

Xuan Tian [a,b,1], Xin Yan [c,1], Nan Zang [a], Wu Duan [a], Tixiao Wang [a], Xiaoxun Li [g], Ling Ma [b], Li Chen [a,d,e,f], Jun Chen [a,**], Xinguo Hou [a,d,e,f,*]

[a] Department of Endocrinology, Qilu Hospital of Shandong University, Jinan, Shandong, 250012, China
[b] Department of Plastic Surgery, Qilu Hospital of Shandong University, Jinan, Shandong, 250012, China
[c] Department of Oncology, Shandong Provincial Hospital Affiliated to Shandong First Medical University, Jinan, Shandong, 250021, China
[d] Institute of Endocrine and Metabolic Diseases of Shandong University, Jinan, Shandong, 250012, China
[e] Key Laboratory of Endocrine and Metabolic Diseases, Shandong Province Medicine & Health, Jinan, Shandong, 250012, China
[f] Jinan Clinical Research Center for Endocrine and Metabolic Disease, Jinan, Shandong, 250012, China
[g] Jinan Aixinzhuoer Medical Laboratory, Jinan, 250100, China

ARTICLE INFO

Keywords:
Limb ischemia
Mesenchymal stem cell
Selenium
Hydrogel

ABSTRACT

Limb ischemia is a refractory disease characterized by persistent inflammation, insufficient angiogenesis, and tissue necrosis. Although mesenchymal stem cells (MSCs) have shown potential for treating limb ischemia, their therapeutic effects are limited by low engraftment rates. Therefore, developing an optimal MSC delivery system that enhances cell viability is imperative. Selenium, known for its cytoprotective properties in various cell types, offers a potential strategy to enhance therapeutic effect of MSCs. In this study, we evaluated the cytoprotective effects of selenium on MSCs, and developed an injectable thermosensitive selenium-containing hydrogel based on PLGA-PEG-PLGA triblock copolymer, as a cell carrier to improve MSC viability after engraftment. The biocompatibility, biodegradability, and cytoprotective capabilities of selenium-containing hydrogels were assessed. Furthermore, the therapeutic potential of MSCs encapsulated within a thermosensitive selenium-containing hydrogel in limb ischemia was evaluated using cellular and animal experiments. Selenium protects MSCs from oxidative damage by upregulating GPX4 through a transcriptional mechanism. The injectable thermosensitive selenium-containing hydrogel exhibited favorable biocompatibility, biodegradability, and antioxidant properties. It can be easily injected into the target area in liquid form at room temperature and undergoes gelation at body temperature, thereby preventing the diffusion of selenium and promoting the cytoprotection of MSCs. Furthermore, MSCs encapsulated within the selenium-containing hydrogel effectively inhibited macrophage M1 polarization while promoting macrophage M2 polarization, thus accelerating angiogenesis and restoring blood perfusion in ischemic limbs. This study demonstrated the potential of an injectable thermosensitive selenium-containing hydrogel as a promising method for MSC delivery. By addressing the challenge of low retention rate, which is a major obstacle in MSC application, this strategy effectively improves limb ischemia.

1. Introduction

Limb ischemia is a severe condition of peripheral arterial disease that affects more than 20 million patients worldwide [1]. This condition is characterized by ischemic pain, ulceration, or gangrene, and ultimately limb amputation and mortality. Despite current therapeutic strategies, including medication to reduce cardiovascular risk, endovascular or surgical treatment to revascularize occluded vessels, and local care to promote healing, complete cure of limb ischemia remains elusive, with limb loss rates as high as 25 % [2]. The inflammatory environment resulting from ischemia induces macrophage M1 polarization, which inhibits angiogenesis and tissue repair, making limb ischemia an

* Corresponding authors. Department of Endocrinology, Qilu Hospital of Shandong University, Jinan, Shandong, 250012, China.
** Corresponding author.
E-mail addresses: junchen001@outlook.com (J. Chen), houxinguo@sdu.edu.cn (X. Hou).
[1] Contributed equally.

https://doi.org/10.1016/j.mtbio.2024.100967
Received 9 November 2023; Received in revised form 13 January 2024; Accepted 19 January 2024
Available online 20 January 2024

intractable problem [3].

Mesenchymal stem cells (MSCs) hold promise as a biological therapy for limb ischemia because of their ability to secrete bioactive and immunomodulatory factors that can reduce M1 polarization and promote M2 polarization [4]. Over 1000 registered clinical trials have explored the use of MSCs (www.clinicaltrials.gov). However, compared to *in vitro* culture, MSCs engrafted at ischemic sites face an inclement microenvironment, including hypoxia and oxidative stress [5]. Hence, reactive oxygen species (ROS) and lipid peroxidation accumulate, which disrupts redox equilibrium and triggers diverse forms of cell death signals, eventually leading to a reduction in the MSC engraftment rate [6,7]. Improving MSC survival in injured tissues represents a prospective approach for enhancing the therapeutic effect of cell-based therapies for limb ischemia.

As an essential trace element, selenium (Se) is crucial for the biosynthesis of selenoproteins, including members of the glutathione peroxidase (GPX) family. These selenoproteins serve as antioxidant enzymes, exhibit potent anti-inflammatory and radical-scavenging properties by reducing H_2O_2 or lipid peroxides, and play a central role in maintaining cellular homeostasis [8]. Sodium selenite (Na_2SeO_3) is used to protect neurons and lymphocytes from ferroptosis [9,10]. Given the cytoprotective effects of Se, it is conceivable that it could act as a protective agent to enhance MSC engraftment efficiency. However, when Se is co-injected with MSCs into the body, it becomes diluted owing to local diffusion, limiting its protective effect. Therefore, the development of a new delivery system that extends the residence time of Se is crucial issue to be solved.

Poly (lactic-*co*-glycolic acid) (PLGA)-poly (ethylene glycol) (PEG)-PLGA is a Food and Drug Administration-approved polymer with excellent biocompatibility, biodegradability, and biosafety. It has been extensively employed for drug encapsulation in a wide range of clinical trials because of its beneficial properties [11]. In this study, we incorporated Se into a PLGA-PEG-PLGA hydrogel to obtain an injectable thermosensitive Se-containing hydrogel as a carrier for MSC. The Se-containing hydrogel remains in solution at room temperature (25 °C), and subsequently turns to gel with a 3D porous network structure after *in vivo* injection (37 °C), which is favorable for ion retention and cell growth. Se trapped within the 3D structure formed homogeneous solid hydrogel electrolytes that were not diluted in the interstitial fluid, thus maintaining an effective local concentration in the long term and exerting antioxidant and pro-survival properties.

Herein, we report that Se supplementation upregulates the expression of selenoproteins, particularly GPX4, in MSCs. Moreover, we demonstrated that the injectable thermosensitive Se-containing PLGA-PEG-PLGA hydrogel was a favorable carrier for MSCs, prolonging the contact time between Se and MSCs at the sites of injury. This approach represents a feasible strategy for improving the therapeutic efficacy of MSCs in the treatment of limb ischemia.

2. Methods

Additional materials and methods are provided in supplemental materials.

2.1. Mesenchymal stem cell isolation

MSCs were isolated from human umbilical cord. A fresh umbilical cord was washed with PBS on a clean laminar flow bench. The umbilical cord adventitia and umbilical vessels were removed to obtain Wharton's jelly. The Wharton's jelly was cut into small pieces and cultured in α-MEM medium (Gibco, NY, USA) containing 10 % FBS (Gibco) at 37 °C in 5 % CO_2. Cell adherence and growth were observed, and the culture medium was changed every 3–4 d. All participants provided informed consent before participation. All protocols were approved by the Ethics Committee of Qilu Hospital of Shandong University (Jinan, China).

2.2. Cell viability

Cell viability was measured using the Cell Counting Kit-8 (CCK-8) (Solarbio, Beijing, China) according to the manufacturer's instructions. In brief, 1×10^4 cells were incubated with 10 μL CCK-8 reagent for 30 min, and optical density (OD) values at 450 nm were measured.

A calcein/PI assay kit (Beyotime, Shanghai, China) was used to simultaneously stain viable and dead cells. Calcein AM/PI assay solution was prepared according to the manufacturer's protocol. The cells were washed twice with PBS and incubated with Calcein AM/PI assay solution at 37 °C for 15 min. Fluorescence was detected using an ECLIPSE Ni fluorescence microscope (Nikon). Cell counting was performed using the ImageJ software.

2.3. Antioxidant capacity assay

The antioxidant capacity was measured using a total antioxidant capacity assay kit according to the ABTS method (Beyotime). The cells (1×10^6) were ultrasonically lysed and centrifuged at 10000 g for 10 min to obtain the supernatant. 20 μL supernatant was incubated with 200 μL ABTS reagent for 15 min. The antioxidant capacity was evaluated by measuring the OD at 414 nm.

2.4. Extraction of RNA and qRT-PCR

Total RNA was extracted using the TRIzol reagent (Takara, Shiga, Japan). Reverse transcription was performed using the PrimeScript RT Reagent Kit (Takara), and qRT-PCR was performed using SYBR Green PCR Master Mix (Takara) according to the manufacturer's instructions. B-actin was used for mRNA standardization. The primer sequences are listed in Table S1.

2.5. Transient transfection

The following small interfering RNAs (siRNAs) were purchased from Thermo Fisher Scientific (Waltham, MA, USA): siGPX4 (10848), siSP1 (116546), siGTF2I (289315), siSRF (115344), siMYB (107687), and siNRF1 (107597). Lipofectamine 3000 (Invitrogen) was used for transient siRNA transfection. Briefly, the cells were seeded in 6-well plates. When the cell confluency reached 70 %, siRNA-lipid complexes were prepared according to the manufacturer's instructions and added to the cells. After 48 h of transfection, siRNA transfection efficiency was evaluated by qRT-PCR and western blotting, and the cells were used for further experiments.

2.6. Extraction, characterization, and protein concentration measurement of exosomes

Exosomes were isolated by differential centrifugation. The exosome-free culture medium was used 48 h before exosome isolation. The cell culture medium was centrifuged at 10000×*g* for 30 min at 4 °C to remove cell fragments, and then the supernatant was centrifuged at 100000×*g* for 70 min at 4 °C to obtain exosomes. The supernatant was discarded, and exosomes were resuspended with PBS and stored at −80 °C. The morphology of the exosomes was observed using a transmission electron microscope (Hitachi, Tokyo, Japan), and the particle size was determined using Nanosight NS300 (Malvern Instruments Ltd., Malvern, UK). An equal volume of RIPA reagent (Beyotime) was added to the exosomes and the protein concentration was measured using a BCA protein assay kit (Beyotime).

2.7. Lipid peroxidation and ROS assay

Cells were dyed with 5 μM BODIPY 581/591 C11 (Thermo Fisher) for 20 min and washed twice in PBS. Lipid reactive oxygen species (ROS) levels were measured by flow cytometry.

The cells were ultrasonically lysed and centrifuged at 10000×*g* for 10 min to collect the supernatant. An MDA assay kit (Beyotime) was used to detect malondialdehyde (MDA) concentration by measuring the OD values at 532 nm according to the manufacturer's instructions.

Intracellular reactive oxygen species (ROS) were measured using a reactive oxygen species assay kit (Beyotime). In brief, cells were incubated with 10 μM fluorescent probe DCFH-DA for 30 min at 4 °C, and washed twice in PBS. Fluorescence distribution was observed using a fluorescence microscope (Nikon). The fluorescence intensity was quantified using ImageJ software.

2.8. Immunofluorescence staining

Cells were fixed in 4 % paraformaldehyde at room temperature for 10 min and permeabilized in 0.25 % Triton X-100 for 10 min, then blocked using 1 % BSA for 30 min and incubated overnight at 4 °C with the GPX4 antibody (Servicebio, Wuhan, China) after 1:500 dilution. The cells were washed twice with PBS and incubated with secondary antibody for 1 h at room temperature. DAPI was used to stain the nuclei. An ECLIPSE Ni fluorescence microscope (Nikon, Tokyo, Japan) was used for visualization. The fluorescence intensity was quantified using ImageJ software.

2.9. Preparation of hydrogels

The PLGA-PEG-PLGA triblock copolymer (1600-1500-1600, cat.15376–372) was purchased from Daigang Biomaterials (Jinan, China) and dissolved in PBS overnight to obtain the PLGA-PEG-PLGA precursor solution. Sodium selenite (cat.10102-18-8) was purchased from Sigma-Aldrich (St. Louis, MO, USA) and added to the PLGA-PEG-PLGA solution by vortexing, followed by 2 h of incubation at room temperature to obtain a Se-containing PLGA-PEG-PLGA solution.

2.10. Cell lines and animals

MH-S cells (a murine alveolar macrophage cell line) and L929 cells (a murine fibroblast cell line) were purchased from Servicebio and cultured in the 1640 medium (Gibco) containing 10 % FBS (Gibco) under standard condition (37 °C and 5 % CO_2). The C57BL/6 mice were purchased from Huafu Kang (Beijing, China). All animal experiments were performed in accordance with current ethical guidelines and approved by the Animal Ethics Committee of Qilu Hospital of Shandong University (Jinan, China).

2.11. Characterization of Se-containing PLGA-PEG-PLGA hydrogel

Gelation temperature: The gelation temperature was determined using a tube inversion test. We heated 1 mL sample in a glass tube from 20 to 60 °C at the rate of 0.5 °C/min. The glass tube was inverted every minute, and the gelation temperature was defined when the gel did not flow down under gravity.

Gelation time: The gelation time was determined using a tube inversion test. 1 mL sample in a glass tube at room temperature was placed in a water bath at 37 °C, and the glass tube was inverted every 5 s. The gelation time was defined when the gel did not flow down under gravity.

Syringeability: The sample was injected through a 25-gauge needle to test the syringeability.

Rheological analysis: Rheological behavior was determined using a rheometer (TA Instruments, New Castle, USA) and heated from 20 °C to 60 °C at a rate of 0.5 °C/min.

Morphological observation: The sample was transferred to a scanning electron microscope (Helios G4 UC, Thermo Fisher) using a cryo-transfer system (PP3010T, Quorum, Knutsford, UK) at −180 °C to observe the surface morphology.

Se release analysis: One gram of Se-containing hydrogel was added to 10 mL PBS (PH 7.4) and incubated for different periods (4, 8, 12, 16, 20, and 24 h). PBS was collected at different time points and centrifuged at 1000×*g* for 5 min. The Se concentration was analyzed using inductively coupled plasma mass spectrometry (iCAP Q, Thermo Fisher). The Se release rate was calculated by dividing the Se content in the PBS by the total Se content in the hydrogel.

2.12. Cytotoxicity test

in vitro biocompatibility of the hydrogels was evaluated using the CCK-8 assay. L929 cells (STCC20025G, Servicebio) were cultured with or without hydrogels in MEM for 3 days. The culture medium was then replaced with fresh MEM, and the CCK-8 reagent was added. After incubation for 30 min, the optical density (OD) was measured at 450 nm using a microplate reader (Multiskan SkyHigh, Thermo Fisher).

2.13. Hemolysis test

Fresh mouse whole blood was centrifuged at 500×*g* for 10 min to obtain red blood cells, and then red blood cells were diluted to 5 % in normal saline. 300 μL red blood cells were mixed with 700 μL hydrogel and incubated at 37 °C for 1 h. The samples were centrifuged at 500×*g* for 10 min. The OD value of the supernatant at 540 nm was measured using a microplate reader (Thermo Fisher Scientific). The hemolysis ratio was calculated by dividing the OD value of the experimental group by the OD value of the positive control (double-distilled water).

2.14. In vitro and in vivo degradation test

1 mL 20 wt% PLGA-PEG-PLGA solution was seeded in a 24 well-plate at 37 °C for gel formation. After gelation, the hydrogel was placed in a cell culture dish and incubated with 10 mL PH 7.4 PBS with collagenase IV (1 μg/mL) at 37 °C for 21 days. At each set time point, the PBS was removed, and the hydrogel was lyophilized and weighed. The degradation ratio was calculated by dividing the weight of the lyophilized hydrogel by that of the PLGA-PEG-PLGA triblock copolymer used to prepare the hydrogel.

For *in vivo* degradation test, 200 μL 20 wt% hydrogel was subcutaneously injected into the inguinal region of the mouse. At each time point, the mice were sacrificed for observation and histological examination.

2.15. In vivo tracking of MSCs encapsulated in the hydrogel

MSCs were dyed with 1 μM CM-Dil dye (Invitrogen) for 30 min, washed using PBS, and centrifuged at 300×*g* for 5 min. CM-Dil dyed MSCs were encapsulated in the hydrogel and subcutaneously injected into the inguinal region of the mice. MSCs were detected using a Maestro *in vivo* imaging system (CRi, Woburn, MA, USA).

2.16. Limb ischemia mouse model

A mouse model of limb ischemia was established as previously described [12]. Briefly, femoral artery ligation and transection were performed to induce limb ischemia, and the contralateral limb was used as a control. All animal experiments were performed in accordance with current ethical guidelines and approved by the Animal Ethics Committee of Qilu Hospital of Shandong University.

2.17. Assessment of limb function

The Tarlov scoring system was used to assess limb function, as previously reported [13]. Tarlov functional scores were defined as follows: 0, no movement; 1, barely observable movement, no weight bearing; 2, frequent and vigorous movement, no weight bearing; 3, supporting weight, may take one or two steps; 4, walking with mild deficit; 5, slow

walking; and 6, normal walking.

2.18. Histology

Muscle tissue fixed in 4 % formalin and embedded in paraffin. 4-μm sections were cut and stained with hematoxylin and eosin (H&E). Masson staining was performed 'using a Masson Staining Kit (Solarbio) according to the manufacturer's instructions.

For immunofluorescence staining, after deparaffinization, antigen retrieval, and blocking, sections were incubated overnight at 4 °C with the following antibodies: CD31 (Servicebio), CD163 (Servicebio), and iNOS (Servicebio) at 1:500 dilution and incubated with the secondary antibody for 1 h at room temperature. An ECLIPSE Ni fluorescence microscope (Nikon) was used for visualization.

2.19. ELISA

100 μL cell culture supernatants were added into the ELISA plates (Abcam, Cambridge, UK) pre-coated with PEG2, TGF-β, IDO, TSG6, TNF-α, IL-1β, and IL-6 antibodies and incubated for 2 h at room temperature. After washing, biotin-labeled detection antibody was added and incubated for 1 h at 37 °C. Avidin-horseradish peroxidase was used for color development. The OD values at 450 nm were measured using a microplate reader (Thermo Fisher Scientific).

2.20. Statistical analysis

Data were presented as mean ± standard deviation. Normality was tested using the Shapiro–Wilk test. Data between two groups were

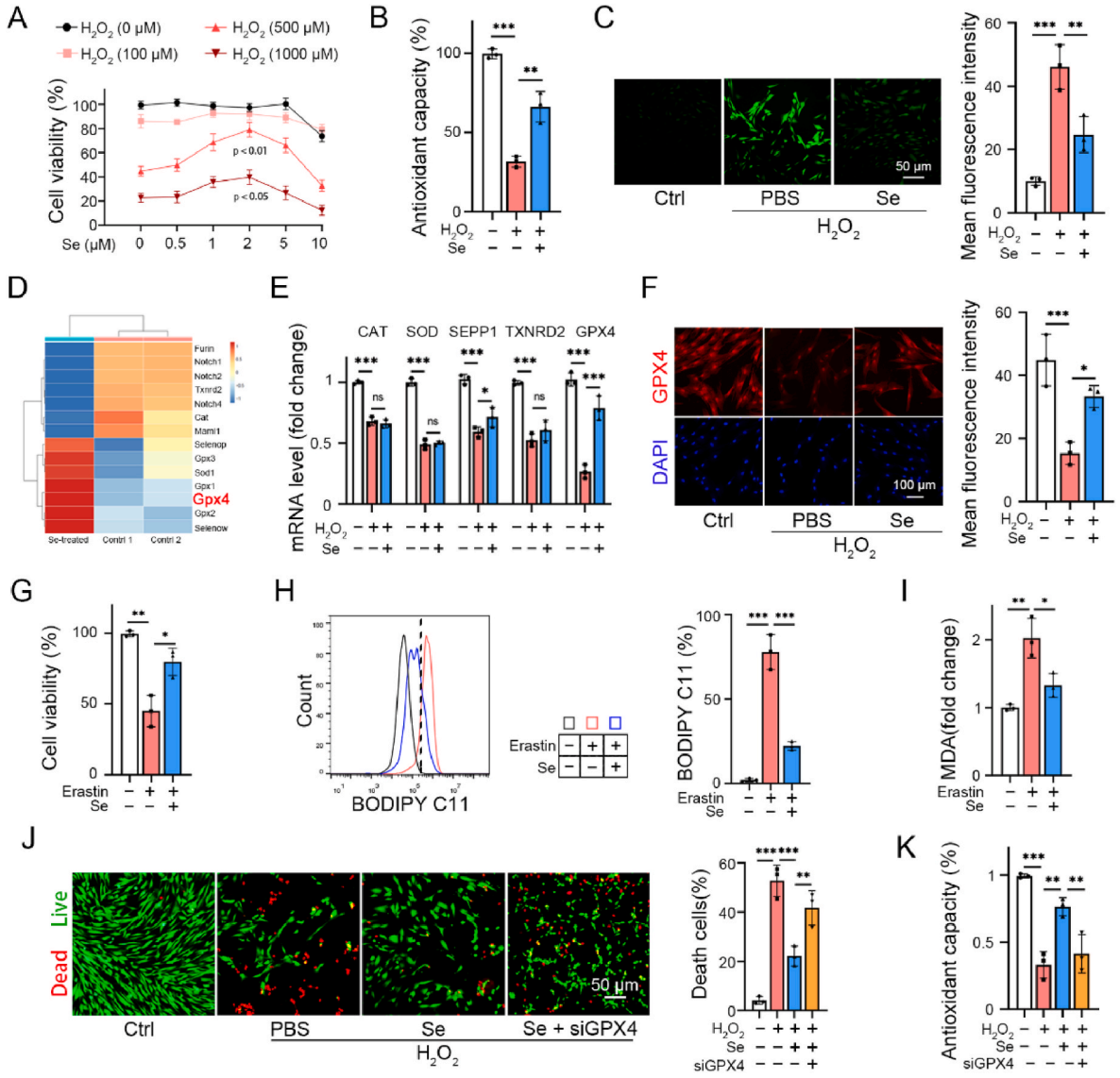

Fig. 1. Se supplementation prevents MSC from oxidative damage.
(A–C) Dose-dependent effect of Se supplementation on viability (A), antioxidant capacity (B), and ROS production (C) of MSCs exposed to H_2O_2 for 24 h (n = 3). (D) Heat map showed that GPX4 was among the most significant DEGs between non-treated controls and Se-treated cells. (E) Protective concentration of Se (2 mM) elevated selenoprotein (especially GPX4) mRNA levels in MSCs exposed to H_2O_2 (500 μM) for 24 h (n = 3). (F) Immunofluorescence staining showed that protein level of GPX4 was augmented by 2 mM Se in MSCs exposed to H_2O_2 (500 μM) for 24 h (n = 3). (G–I) MSCs were treated with Erastin (10 μM) in presence or absence of Se (2 mM) for 24 h. Se increased cell viability measured by a CCK-8 kit (F), and suppressed Erastin-induced lipid ROS dyed using BODIPY C11 (G) and lipid peroxidation measured by an MDA assay kit (H) (n = 3). (J) Live(green)/Dead (red) assay showed that GPX4 silencing by siRNA counteracted protection of Se (2 mM) and enhanced cell death (n = 3). (K) Total antioxidant capacity was assayed with an ABTS method, and GPX4 silencing abrogated antioxidation effect of Se (2 mM) (n = 3). * $p < 0.05$, ** $p < 0.01$, *** $p < 0.001$, ns = no significance. (For interpretation of the references to colour in this figure legend, the reader is referred to the Web version of this article.)

analyzed using the Student's t-test, and data among three or more groups were analyzed using one-way ANOVA. All data were analyzed and visualized using GraphPad Prism 9 (San Diego, CA, USA). $p < 0.05$ was considered to be statistically significant.

3. Results

3.1. Selenium protects MSCs from oxidative damage

Se is essential for the biosynthesis of antioxidative selenoproteins and plays a crucial role in scavenging ROS and maintaining redox equilibrium [14]. Accordingly, we isolated MSCs from the human umbilical cord (Fig. S1) and investigated whether Se supplementation protected MSCs from oxidative damage (Fig. 1 A).

Our analysis revealed that H_2O_2 induced cell death within the concentration range of 100–1000 μM, while Se supplementation conferred a dose-dependent protective effect on MSCs within the concentration range of 0–2 μM (Fig. 1 A). Since Se treatment at concentrations higher than 2 μM exhibited cytotoxicity, we chose 2 μM as the concentration of Se for subsequent experiments. Notably, supplementation with 2 μM Se significantly rescued the decrease in antioxidant ability and reduced ROS production induced by H_2O_2 (Fig. 1 B, C). RNA-seq data (GSE148673) were analyzed and GPX4 was found to be among the most significantly differentially expressed genes (DEGs) between non-treated controls and Se-treated cells (Fig. 1 D, Fig. S2 A). Antioxidant activity, transcription coregulatory activity, and transcription coactivator activity were enriched in the DEGs (Fig. S2 B-D). Next, the mRNA levels of some major antioxidases were measured. The results showed that Se increased the expression of Se-containing antioxidases, especially GPX4, rather than Se-free antioxidases, indicating that GPX4 may be the main executor of antioxidation following Se treatment (Fig. 1 E). Se consistently induced a robust increase in GPX4 protein levels (Fig. 1 F). Erastin is a ferroptosis inducer that induces cell death through antioxidant depletion and GPX4 degradation [15]. We found that Se also reduced erastin-induced mortality and ferroptosis biomarkers, such as lipid ROS and MDA, in MSCs (Fig. 1G–I).

To further confirm the pivotal role of Se-induced GPX4 expression in cytoprotection, we knocked down GPX4 using a specific small interfering RNA (siRNA), and evaluated the knockdown efficiency using qRT-PCR and western blotting (Fig. S3). GPX4 knockdown abrogated the protective effect of Se supplementation against H_2O_2-induced cell death and decreased antioxidant ability (Fig. 1 J, K).

Collectively, these results demonstrate that Se could serve as a novel protective agent with powerful antioxidant effects, providing a new possibility for enhancing MSC viability.

3.2. Selenium protects MSCs against oxidative damage through regulating GPX4 transcription

To further investigate the involvement of Se in the transcription of GPX4, we treated MSCs under oxidative pressure with Se followed by treatment with the transcription inhibitor Actinomycin D (Act D). The results showed that Se increased GPX4 expression in mRNA level, but this upregulation was abrogated by Act D (Fig. 2 A), suggesting that Se exerts a protective effect against oxidative damage by regulating GPX4 transcription.

We then collected transcription factors (TFs) potentially regulated by Se, according to previously published studies (Table S2) [10,16,17]. To identify the TFs regulated by Se that can modulate the transcription of GPX4, we screened the hTF target database (http://bioinfo.life.hust.edu.cn/hTFtarget) (Table S3) [18] and performed Venn diagram analysis, which identified five TFs (SP1, GTF2I, SRF, MYB, and NRF1) (Fig. 2 B).

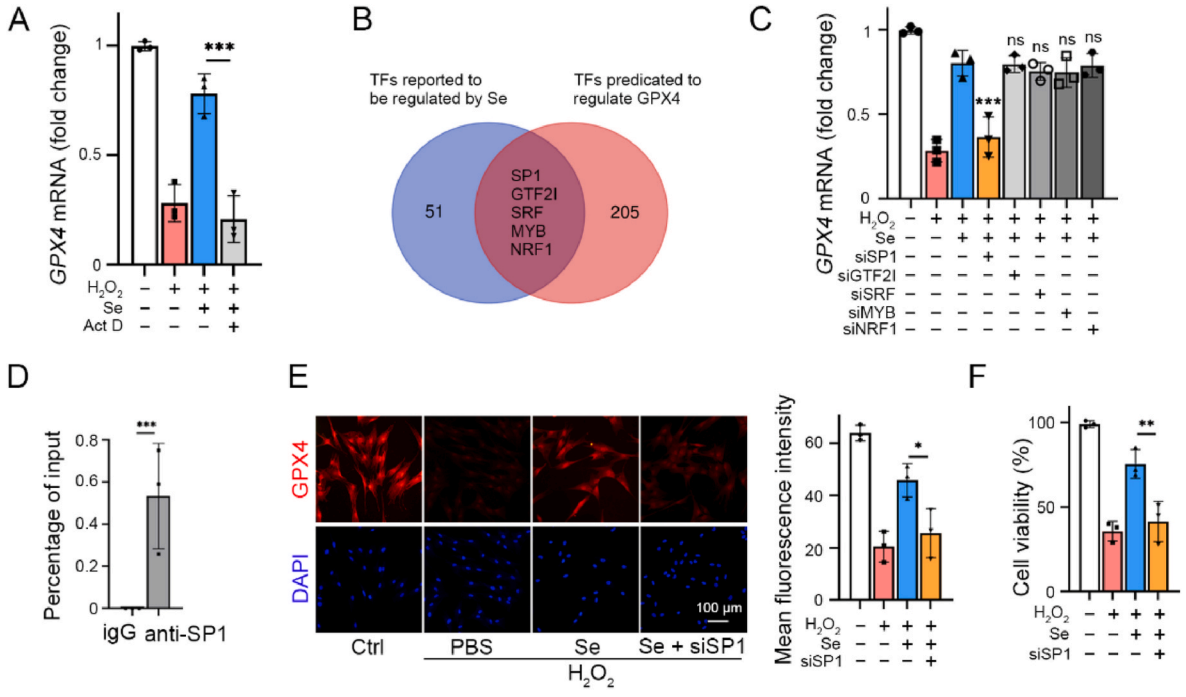

Fig. 2. Effects of Se supplementation on GPX4 transcription.
(A) Transcription inhibitor Act D (2 mg/mL) abrogated Se-induced increasing GPX4 mRNA level in MSCs (n = 3). (B) 56 TFs were potentially regulated by Se referring to published studies, and 210 TFs were predicted to modulate GPX4 transcription using hTFtarget. Intersection between the two TF subsets contained 5 TFs, which were supposed to be potential TFs for Se to regulate GPX4 transcription. Venn diagram was drawn using Universiteit Gent (https://bioinformatics.psb.ugent.be/webtools/Venn/). (C) The 5 TFs were knocked down respectively in MSCs, which were exposed to H_2O_2 (500 μM) with the presence of Se (2 μM) for 24 h. GPX4 mRNA level was measured by qRT-PCR. SP1 knock-down decreased mRNA level of GPX4 (n = 3). (D) ChIP-qPCR analysis of SP1 direct binding to the promoter region of GPX4 (n = 3).(E, F) SP1 was knocked down in MSCs, which is followed by exposure to H_2O_2 (500 μM) with the presence of Se (2 μM) for 24 h. GPX4 protein level was measured by immunofluorescent staining (E), and cell viability was measured by a CCK-8 kit (F). SP1 knock-down decreased the protein level of GPX4 and abrogated protection effect of Se (n = 3).* $p < 0.05$, ** $p < 0.01$, *** $p < 0.001$, ns = no significance.

These five TFs were knocked down using siRNAs, and the knockdown efficiencies were evaluated using qRT-PCR and western blotting (Fig. S3). The results revealed that Se-induced GPX4 transcription was only inhibited by SP1 knockdown (Fig. 2 C). Chromatin immunoprecipitation (ChIP)- qPCR confirmed that SP1 could bind to the promoter region of GPX4 (Fig. 2 D). Moreover, SP1 knockdown reduced the protein levels of GPX4 and abolished the cytoprotective effects of Se supplementation (Fig. 2 E, F). Thus, we demonstrated that Se induces GPX4 expression to protect MSCs from oxidative damage by modulating transcription factor SP1.

3.3. *Preparation and characterization of Se-containing PLGA-PEG-PLGA hydrogel*

To the best of our knowledge, no Se-containing hydrogel is currently used for MSC delivery in limb ischemia treatment. In the present study, we developed a novel Se-containing hydrogel as an MSC carrier. The PLGA-PEG-PLGA hydrogel is a suitable biomaterial with a porous network structure that allows the encapsulation of Se within limiting pores, thereby retarding rapid diffusion. In this study, we prepared PLGA-PEG-PLGA hydrogel (hereinafter referred to as Gel) and Se (2 μM)-containing PLGA-PEG-PLGA hydrogel (hereinafter referred to as Se/Gel) with mass fractions of 15 wt%, 20 wt%, and 25 wt%. The solution-gel transition temperature windows of the Gel and Se/Gel were measured (Fig. 3 A). When temperature increased from 20 °C to 60 °C, the Gel and Se/Gel existed in three states: solution, gel, and suspension. The addition of Se (2 μM) did not significantly affect the gelation property of Gel. Gel and Se/Gel with a mass fraction of 20 wt%, which exhibited a solution-gel transition temperature of approximately 33 °C, were chosen for further experiments due to their convenience for MSCs incorporation at room temperature and gelation upon injection into the body, making them suitable for clinical application.

Syringeability of 20 wt% Gel and Se/Gel at room temperature (25 °C) was high (Fig. 3 B), and their gelation time at body temperature (37 °C) was 66.00 ± 5.56 s and 67.33 ± 5.69 s respectively (Fig. 3 C). After gelation, the Gel and Se/Gel adhered to the tissue and deformed to comply with the muscle contraction without breaking or peeling off, indicating that these hydrogels had flexible mechanical properties to fit muscle movements (Fig. 3 D). Both Gel and Se/Gel transitioned from an aqueous solution to a gel as the temperature increased from room temperature (25 °C) to body temperature (37 °C), suggesting that supplementation of Se did not significantly affect gelation properties (Fig. 3 E). The rheological properties of the Gel and Se/Gel were analyzed using a rheometer (Fig. 3 F). The observation that the storage modulus (G′) was higher than the loss modulus (G') indicated transformation of the solution into a hydrogel. The surface morphologies of the Gel and Se/Gel exhibited 3D porous network structures (Fig. 3 G). Se release rate within 24 h of Se/Gel remained at 27.67 % ± 2.52 %, indicating that Se/Gel had a good in situ retention property of Se (Fig. 3 H).

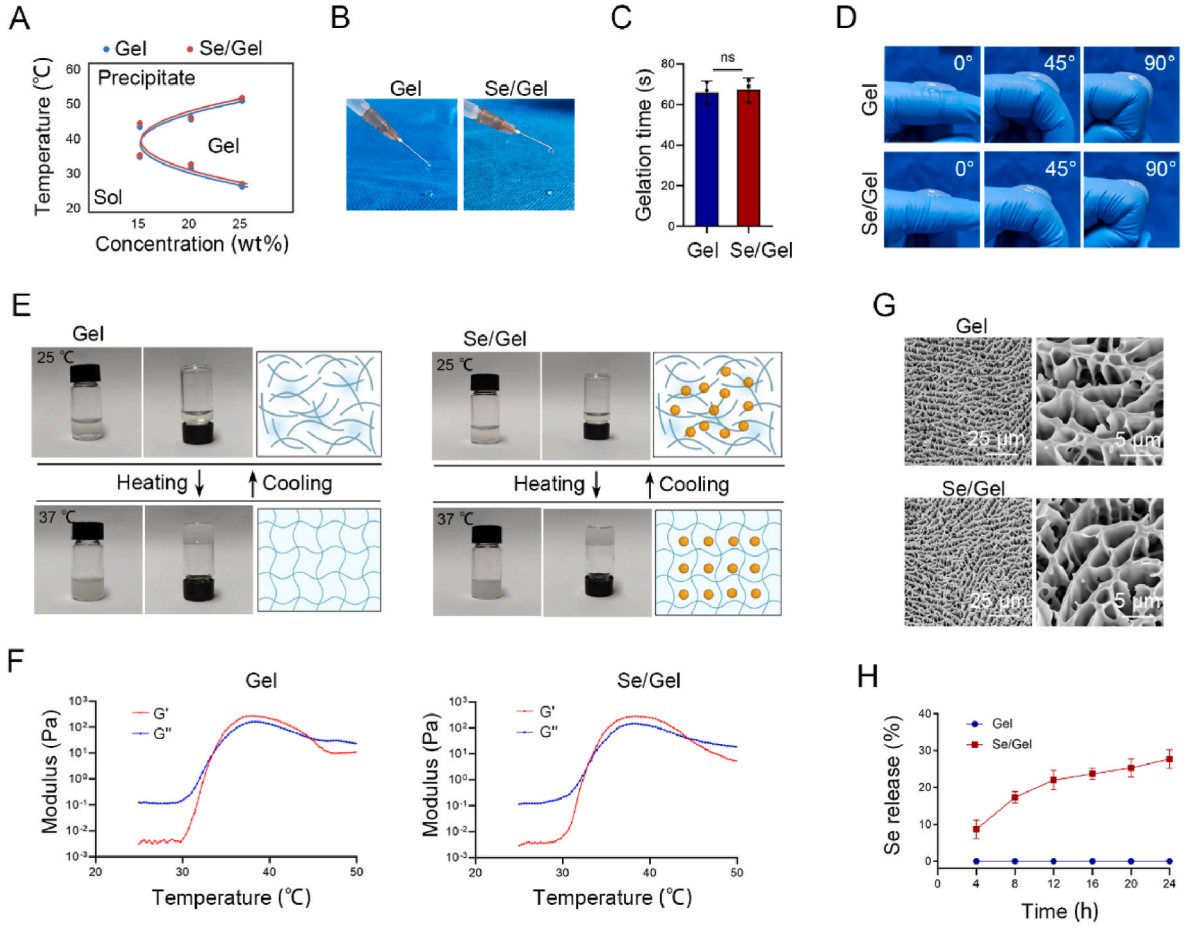

Fig. 3. Characterization of Se-containing PLGA-PEG-PLGA hydrogel.
(A) Phase diagram showed the triphase transformation of the Gel and Se/Gel (15, 20, and 25 wt%). (B) Representative images showed syringeability of the Gel and Se/Gel (20 wt%). (C) Gelation time at 37 °C of the Gel and Se/Gel (20 wt%). (D) Mechanical property of the Gel and Se/Gel (20 wt%). (E) Representative pictures and schematic diagrams showed gross morphology of thermosensitive solution–gel transition of the Gel and Se/Gel (20 wt%). (F) Rheological behavior of the Gel and Se/Gel (20 wt%). (G) Representative TEM images showed micromorphology of the Gel and Se/Gel (20 wt%). (H) Se release curve from the Gel and Se/Gel in PBS of pH 7.4 within 24 h.

3.4. In vitro and in vivo biocompatibility of Se-containing hydrogel

To evaluate the cytotoxicity of the novel Se/Gel, L929 cells were cultured in 96-well plates, and the cell viability was measured with or without Se/Gel seeded on the surface (Fig. 4 A). The results showed that the addition of Se/Gel did not exert a significant effect on the proliferative activity (Fig. 4 B). *in vitro* hemolysis test was conducted to further evaluate the biocompatibility of the Se/Gel. Hemolysis ratios of the Gel and Se/Gel were all below 5 % compared to the positive control (double distilled water) (Fig. 4 C, D). Furthermore, *in vitro* and *in vivo* degradation tests were conducted to evaluate the use of Se/Gel as a local implant material (Fig. 4E–G). *in vitro* degradation ratios of the Gel and Se/Gel did not differ significantly, and reached 82.33 ± 3.05 % and 81.67 ± 6.80 % respectively after 21 days (Fig. 4 E). The *in vivo* degradation test showed that Gel and Se/Gel gradually degraded over time during the 21-day observation period (Fig. 4 G). Histological examinations were conducted to evaluate the inflammatory response induced by the hydrogels (Fig. 4 H, I), and there was no significant difference in the number of infiltrated inflammatory cells at the hydrogel injection site between the Gel and the Se/Gel. The results revealed noticeable inflammatory cell infiltration in the surrounding subcutaneous tissues at 7 and 14 days after injection of the Gel and Se/Gel. However, the inflammatory response was markedly attenuated on the 21st day, as the hydrogels degraded. Together, these results demonstrate the good tissue compatibility of the Se/Gel.

3.5. Se-containing hydrogel enhances survival and improves immunoregulatory capability of MSCs under oxidative pressure

Fig. S4MSCs were encapsulated in a PLGA-PEG-PLGA hydrogel (to obtain Gel/MSC) or Se-containing PLGA-PEG-PLGA hydrogel (to obtain Se/Gel/MSC) at a density of 1×10^6 cells/mL, as shown in Fig. 5 A. We found that the viability of Se/Gel/MSC under oxidative pressure induced by H_2O_2 or Erastin reached 72.01 ± 6.03 % and 78.33 ± 7.57 %, respectively, compared to 35.67 ± 9.79 % and 47.33 ± 11.06 % for Gel/MSC (Fig. 5 B), indicating that Se/Gel exerted a potent cytoprotective effect against oxidative damage.

Exosomes derived from Gel/MSC or Se/Gel/MSC were extracted and characterized (Fig. 5 C), and the concentration of exosomal proteins was measured to evaluate the paracrine activities of MSCs (Fig. 5 D). In the Gel/MSC group, the concentration of exosomal proteins decreased by nearly three-quarters under oxidative pressure, whereas Se/Gel encapsulation significantly improved the paracrine activity of MSCs by more than 3 folds compared to gel encapsulation (Fig. 5 D). Furthermore, the

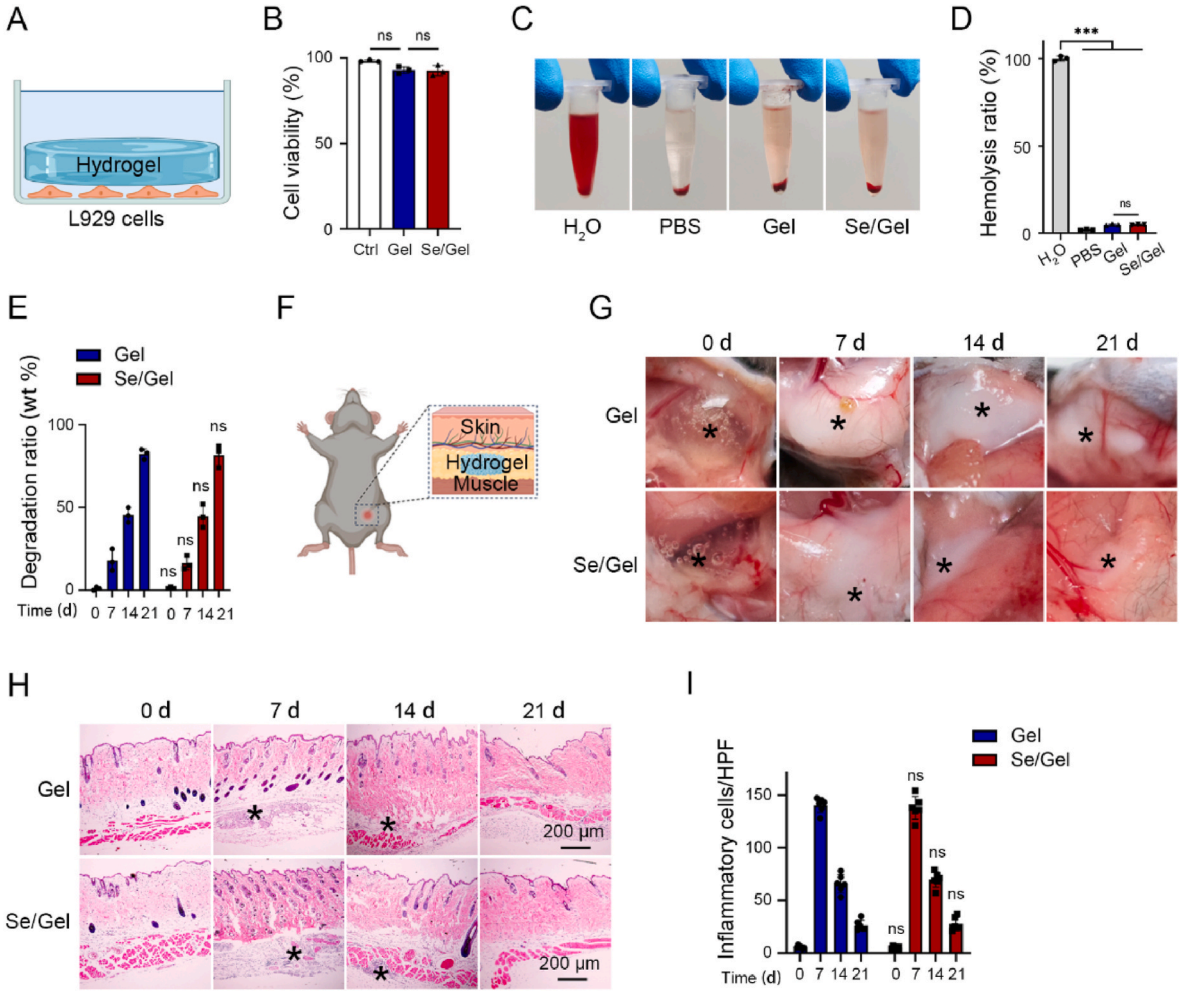

Fig. 4. Biocompatibility of Se/Gel *in vitro* and *in vivo*
(A) Schematic illustration of *in vitro* biocompatibility test. (B) MSC viability measured by CCK-8 assay after incubation with or without hydrogels seeded on the surface for 3 days (n = 3). (C, D) Photographs (C) and statistical data (D) of hemolytic effects of the hydrogels (n = 3). (E) Degradation ratios of the hydrogels in pH 7.4 PBS with collagenase IV (1 μg/mL) at 37 °C (n = 3). (F) Schematic illustration of *in vivo* biocompatibility test. (G) Gross observation of the hydrogels after subcutaneously injection at different time points (n = 3). (H) Histological examination of tissues at the hydrogel injection site (n = 3). The asterisk indicates inflammatory cell infiltration. (I) Quantitative data of infiltrated inflammatory cells per high-power field at the hydrogel injection site.*** $p < 0.001$, ns = no significance.

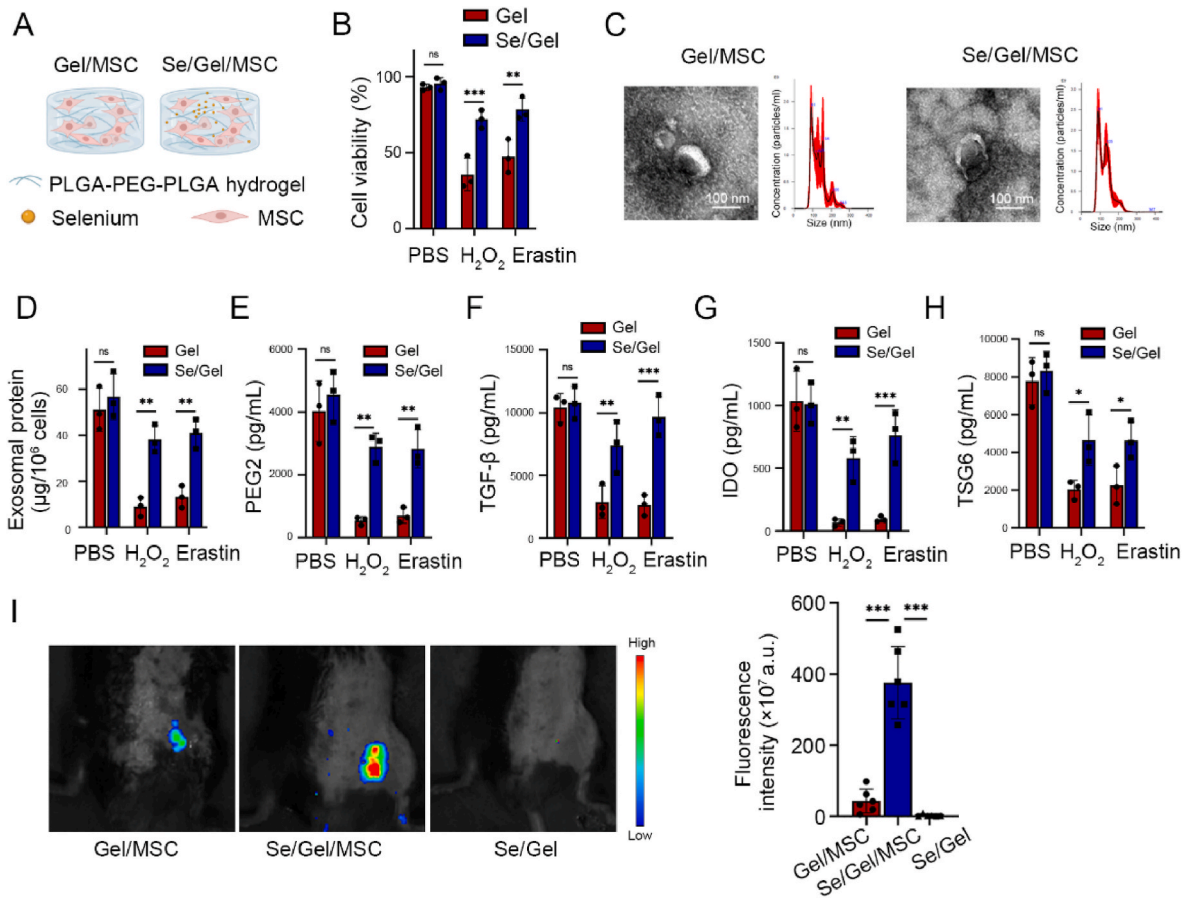

Fig. 5. Effects of Se/Gel on viability and immunoregulatory capability of MSCs.
(A) Schematic illustration of MSCs encapsulated in the Gel and Se/Gel. (B) Viability of MSCs encapsulated in the Gel or Se/Gel under oxidative pressure induced by H_2O_2 (500 μM) or Erastin (10 μM) for 24 h (n = 3). (C) Exosomes of MSCs encapsulated in the Gel or Se/Gel were isolated by ultracentrifugation method after exposure to H_2O_2 or Erastin for 48 h. The morphology of exosomes was observed using transmission electron microscope (TEM), and the size of exosomes was measured using nanoparticle tracking analysis (NTA). (D) Exosomal protein concentration was determined by the BCA method (n = 3). (E–H) Immunomodulatory factors including PEG2 (E), TGF-β (F), IDO (G), and TSG6 (H) in culture supernatant of MSCs encapsulated in the Gel or Se/Gel were measured using an ELISA assay after exposure to H_2O_2 or Erastin for 48 h (n = 3). (I) CM-Dil dyed MSCs were encapsulated in the Gel or Se/Gel, and tracked using a Maestro *in vivo* imaging system 24 h after subcutaneous injection (n = 6).* $p < 0.05$, ** $p < 0.01$, *** $p < 0.001$, ns = no significance.

immunomodulatory factors secreted by MSCs were measured. The results showed that both H_2O_2 or Erastin exposure dramatically decreased the secretion of immunomodulatory factors by Gel/MSC, but additional Se counteracted this inhibitory effect (Fig. 5E–H). Finally, *in vivo* tracking of MSCs encapsulated in the hydrogels showed that the Se/Gel increased cell residence at the site of injection compared with the Gel (Fig. 5 I). These observations suggest that the Se/Gel possesses the pivotal advantages of pro-survival and improved immunoregulatory capabilities of MSCs.

3.6. MSCs delivered by Se/gel improved blood perfusion in limb ischemia mouse model

Intravenous supplementation with selenium did not protect the MSCs or directly improve limb ischemia (Fig. S4). Thus, the Se-containing hydrogel was created to enhance the curative effect of MSCs. To evaluate the *in vivo* therapeutic potential, a mouse model of limb ischemia was established, and MSCs encapsulated in the Se/Gel were subcutaneously injected into the injured site (Fig. 6 A). Blood perfusion was monitored during the 21-day observation period (Fig. 6 B). Laser speckle imaging showed that blood flow signals in the injured limb were barely detectable immediately after femoral artery transection. On the 7th day and 21st day, blood perfusion in the ischemic limb exhibited significant restoration following treatment with Se/Gel/MSC compared with both Gel/MSC and Se/Gel (Fig. 6 C, D). Correspondingly, Se/Gel/MSC administration significantly improved limb function (Fig. 6 E). Histological examination revealed focal necrosis and obvious inflammatory cell infiltration in the muscle tissues treated with Gel/MSC or Se/Gel. In contrast, less necrosis and inflammatory cell infiltration were observed when the mice were treated with Se/Gel/MSC (Fig. 6 F). Masson staining was used to distinguish between the collagen and muscle tissues. The results showed abundant collagen formation in the muscle samples of the Se/Gel group, with a reduction in collagen formation after Gel/MSC treatment, and a further significant reduction after Se/Gel/MSC treatment (Fig. 6 G). CD31 immunofluorescence staining demonstrated that Se/Gel/MSC treatment led to the greatest increase in capillary density compared with the other two groups (Fig. 6 H). Correspondingly, *in vitro* scratch assay revealed that the Se/Gel/MSC promoted the proliferation and migration of human umbilical vein endothelial cells (Fig. S5). These findings indicate that MSCs delivered by the Se/Gel effectively attenuated tissue damage induced by ischemia and increased the formation of capillaries, thereby promoting the restoration of limb ischemia.

3.7. MSCs encapsulated in Se/Gel inhibited M1 macrophage polarization and promoted M2 macrophage polarization

We next investigated the potential immunoregulatory activity of

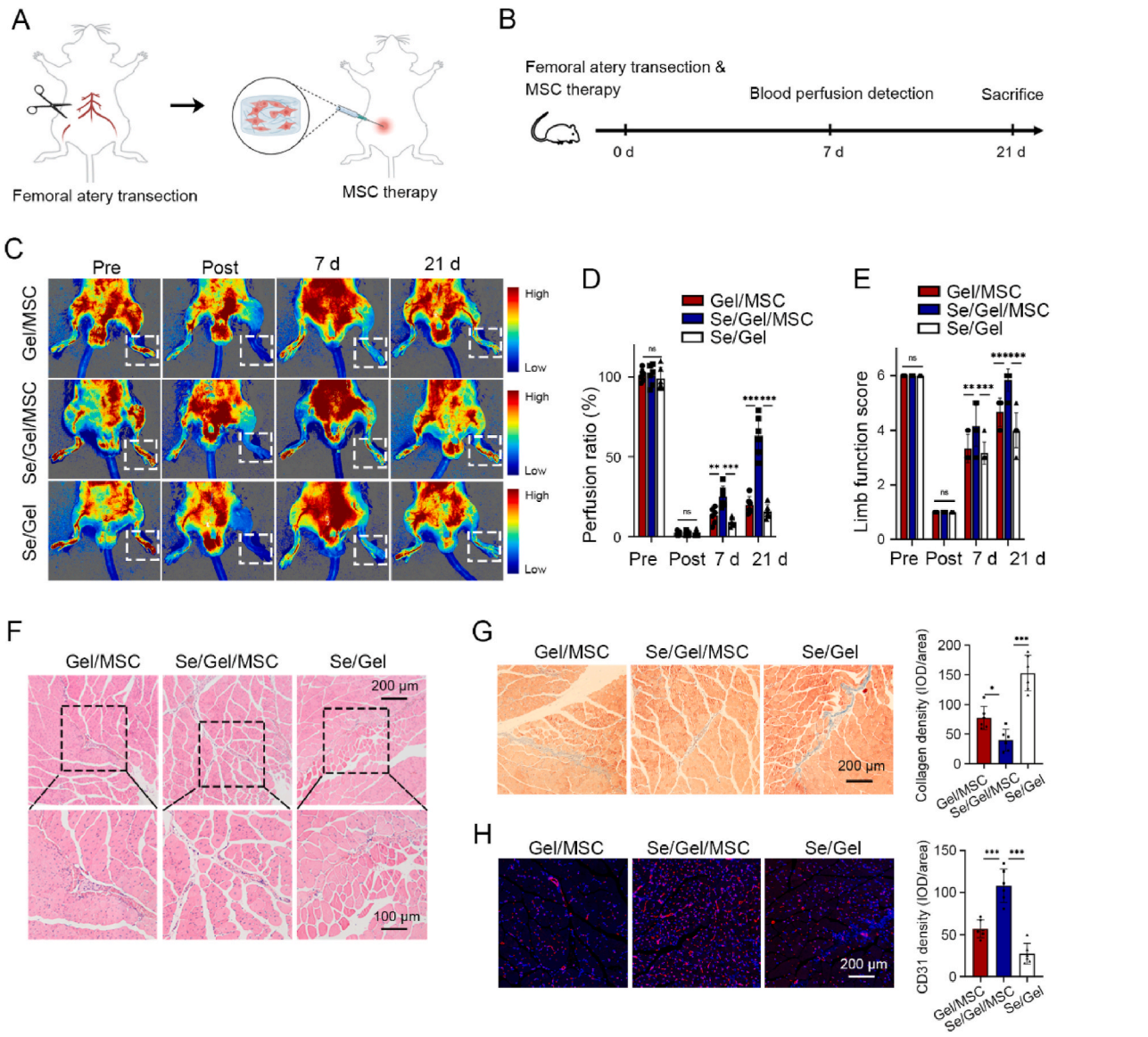

Fig. 6. MSCs encapsulated in Se/Gel improved blood perfusion of limb ischemia.
(A) Schematic illustration of limb ischemia mouse model establishment and hydrogel-encapsulated MSC therapy. (B) Schematic timeline diagram of animal experiments. (C) Representative laser speckle images of limb perfusion in limb ischemia mice model treated with Se/Gel/MSC or Gel/MSC. Se/Gel injection without MSC was used as the control group (n = 6). (D) Quantitative data of blood perfusion measured by the laser speckle imager. (E) Limb function assessed using Tarlov score system. 6 represents normal limb function, and 0 represents limb non-function. (F)Representative H&E staining images of muscle tissues on the 21st day (n = 6). (G) Representative Masson staining images of muscle tissues on the 21st day (n = 6). (H) Representative CD31 immunofluorescence staining images of muscle tissues on the 21st day and quantitative data (n = 6).* $p < 0.05$, ** $p < 0.01$, *** $p < 0.001$, ns = no significance.

MSCs encapsulated in the Se/Gel. Macrophages exhibit high plasticity and tend to polarize into the proinflammatory M1 type when exposed to inflammatory stimuli. M1 macrophages secrete pro-inflammatory cytokines that aggravate inflammatory responses and induce tissue damage, whereas M2 macrophages exert anti-inflammatory effects that promote angiogenesis and tissue regeneration. Immunofluorescence staining revealed a decrease in iNOS + M1 macrophages and an increase in CD163+ M2 macrophages after Se/Gel/MSC or Gel/MSC treatment compared to the Se/Gel group, with the Se/Gel/MSC group showing the most significant therapeutic effect (Fig. 7 A).

To further verify immunomodulatory activity of the Se/Gel/MSC, a transwell system was used to coculture of hydrogel-encapsulated MSCs with macrophages under LPS and IFN-γ stimuli (Fig. 7 B). Pro-inflammatory cytokines, including TNF-α, IL-1β, and IL-6 secreted by macrophages were reduced by Gel/MSC, and further reduced by Se/Gel/MSC (Fig. 7C–E). Immunofluorescence staining showed that M1 polarization was inhibited and M2 polarization was enhanced in the Se/Gel/MSC group compared to the Se/Gel and Gel/MSC groups, indicating that MSCs encapsulated in the Se/Gel possessed more potent immunoregulatory activity (Fig. 7F and G).

4. Discussion

Improving cell survival rate after engraftment has long been a challenge in the application of MSCs. To address this issue in the context of limb ischemia, we present the first study to apply an injectable thermosensitive Se-containing hydrogel as a cell carrier to improve the MSC retention rate. This biocompatible Se-containing hydrogel provides a beneficial niche for MSC survival and immunoregulatory factor secretion, ultimately improving blood perfusion in ischemic limbs.

Selenium is widely recognized as an indispensable trace element with excellent antioxidant properties and protective effects in various

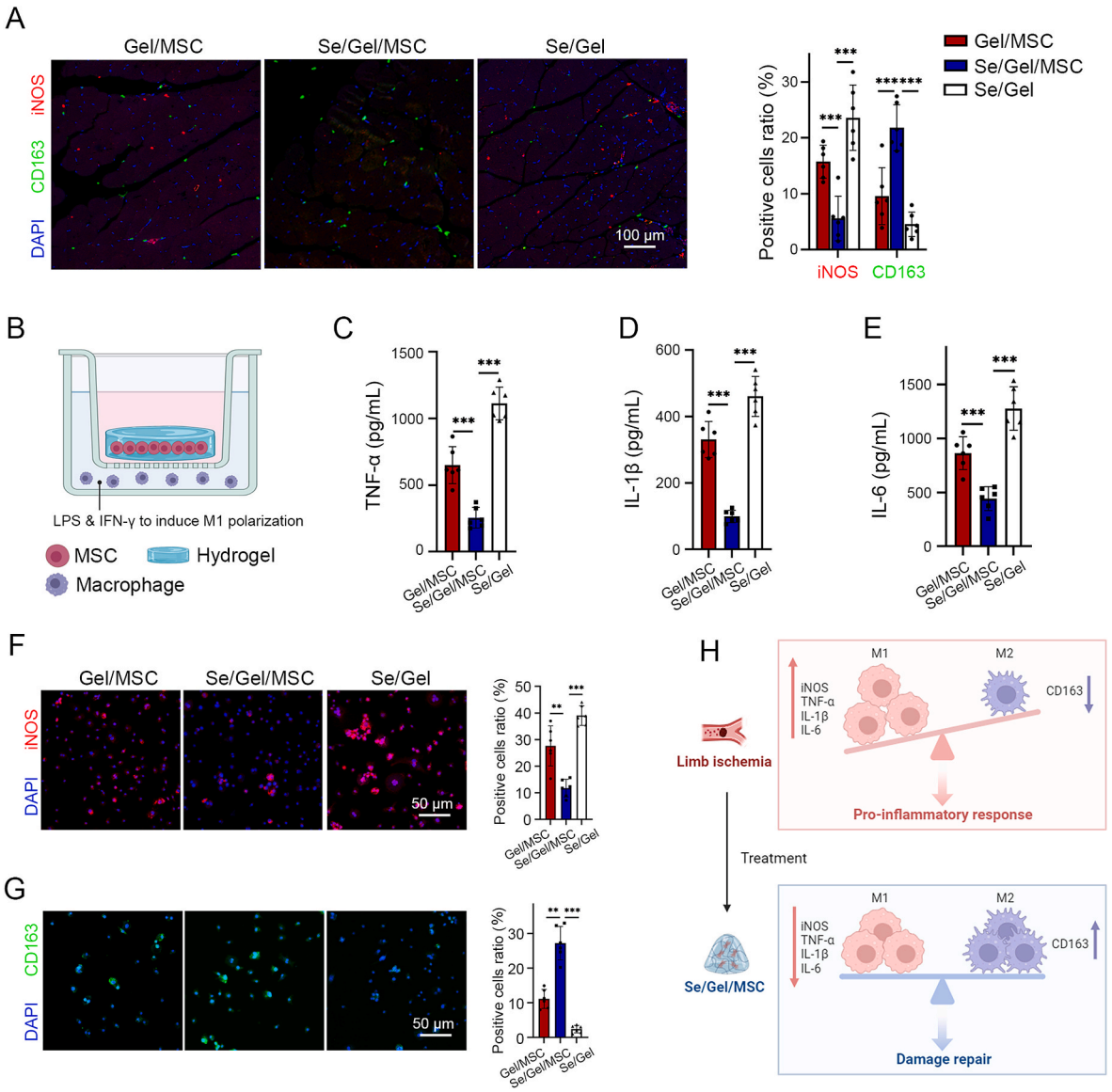

Fig. 7. Immunomodulatory effect of MSCs encapsulated in Se/Gel.
(A) Representative immunofluorescence staining images and quantitative analysis of iNOS + M1 macrophages (red) and CD163+ M2 macrophages (green) of muscle tissues in limb ischemia mouse (n = 6). (B) Schematic illustration of coculture transwell system of macrophages with MSCs encapsulated in hydrogels. (C–E) Macrophages and MSCs encapsulated in hydrogels were cocultured for 96 h under inflammatory condition induced by LPS and IFN-γ stimuli. Pro-inflammatory cytokines including TNF-α(C), IL-1β (D), and IL-6 (E) in culture supernatant were measured using an ELISA method (n = 3). (F, G) Representative immunofluorescence staining images and quantitative analysis of iNOS + M1 macrophages (red) (F) and CD163+ M2 macrophages (green) (G) after 96 h coculture (n = 3). (H) Schematic illustration of immunomodulatory effect of MSCs encapsulated in the Se/Gel on limb ischemia.* $p < 0.05$, ** $p < 0.01$, *** $p < 0.001$, ns = no significance. (For interpretation of the references to colour in this figure legend, the reader is referred to the Web version of this article.)

cell types, including hepatocytes, neurons, immune cells, and kidney tubular cells [19]. Based on these properties, we hypothesized that Se could serve as a protective agent against MSCs. However, the dual character of selenium presents a challenge, as it is an essential microelement at low doses but becomes extremely toxic at high doses [8]. To determine the optimal Se concentration that provides cytoprotective effects with minimal toxicity, we first examined the effect of different Se concentrations on MSCs under oxidative stress. Our results demonstrated that selenium exerts considerable antioxidative effects on MSCs at the concentration of 2 μM, while higher concentrations >5 μM exhibit cytotoxicity, with clear toxicity observed at 10 μM. These findings concur with previous studies which showed that 5 μM selenium induced apoptosis in cervical cancer cells, 7 μM selenium was implicated in cell death of malignant glioma cells, and 20 μM selenium led to apoptosis in leukemia cells [20], although different cells showed virous susceptibilities to selenium.

At protective concentrations, selenium is co-translationally incorporated into the selenoprotein structure in the form of selenocysteine, and the consequences of selenium supplementation depend on the expression levels of selenoproteins [21]. It has been reported that the expression of certain selenoproteins, such as GPX4, is a priority in cases of selenium insufficiency [8]. Consistent with previous research, our study demonstrated that GPX4 was the most significantly increased selenoprotein in response to selenium. Notably, Se supplementation enhanced the transcriptional activity of GPX4. However, the mechanism by which Se, an integral part of GPX4, affects transcription remains to be investigated. To clarify the implications of our findings, we analyzed the relationship between transcription factors potentially modulated by selenium and GPX4 transcription. Further ChIP-qPCR confirmed that SP1 binds directly to the promoter region of GPX4 and promotes

transcription in response to Se supplementation. And it is possible that SP1 is able to perceive Se concentration and sequentially activate GPX4 transcription to exert protection against oxidative stress [10]. We found that selenium promoted GPX4 expression by modulating the transcription factor SP1, representing a novel mechanism by which selenium exerts cytoprotective effects on MSCs under oxidative stress.

Several studies have reported that Se enhances the proliferation, paracrine activity, multipotency, cytoprotective ability, and immunomodulatory ability of MSCs [22–26]. However, when selenium is injected *in vivo* along with MSCs, it is diluted in the interstitial fluid, potentially reducing its efficacy. Maintaining selenium at an optimal local concentration remains a challenge.

To address this challenge, a wide range of hydrogels have been used for the delivery of therapeutic agents, including chitosan hydrogels, sodium alginate hydrogels, gelatin/methacrylic anhydrides, and hyaluronic acid-based hydrogels [27,28]. The PEG–PLGA–PEG triblock copolymer has been approved by the FDA as a biodegradable, non-toxic, and safe biomaterial and has attracted extensive interest in drug delivery research [29]. Compared with other hydrogels, the PLGA hydrogel has several advantages, such as its ability to exist as a solution below the gelation temperature, enabling the incorporation of drugs or cells, and its transformation into a gel with controlled release properties above the gelation temperature. Additionally, the porous structure of the PEG–PLGA–PEG hydrogel provides a favorable niche for cell adhesion and substance exchange.

In this study, physically entrapped selenium was slowly released by diffusion, thus maintaining a considerable local drug concentration around the MSCs. Our study demonstrated that over 70 % of selenium remained trapped within the porous hydrogel after 24 h of incubation in the PBS. We found that the Se-containing PLGA-PEG-PLGA hydrogel had superior cytoprotective efficacy against MSCs compared to the Se-free hydrogel. In addition to enhancing survival, our study also demonstrated that the Se-containing hydrogel modulated the cell behavior of MSCs, including their paracrine activity, proangiogenic ability, and immunoregulatory capacity. *In vitro* results showed that the Se-containing hydrogel increased exosome production and cytokine secretion, through which MSCs exerted therapeutic effects [30]. Through intercellular communication, MSCs interact with neighboring vascular endothelial cells, activate angiogenic signaling pathways, interact with macrophages, and induce M2 polarization to promote tissue repair [31,32]. In summary, these properties provide favorable conditions for perfusion restoration, making the application of MSCs encapsulated in Se-containing hydrogels an attractive strategy for the treatment of limb ischemia.

Furthermore, this injectable in situ forming hydrogel offers the advantage of a minimally invasive injury-targeted cell implantation system with enhanced efficacy and reduced side effects. Intravenous injection of MSCs often results in the majority becoming trapped in lung capillaries, with only a small fraction passing through the lung barrier and migrating to injured organs [33]. This thermosensitive injectable hydrogel makes injury-targeted cell delivery feasible. In this system, MSCs are physically encapsulated in an aqueous Se-containing PLGA--PEG-PLGA solution at room temperature and subsequently injected into a specific injured site to form a stable cell scaffold. This approach enabled a higher MSC concentration than local or intravenous injections, partially addressing the low retention rate of MSCs *in vivo*.

However, it is important to acknowledge the dual effects of Se supplementation. Excess Se can induce DNA damage, oxidative stress, and neurotoxicity in a dose-dependent manner [34]. The beneficial and toxic effects of selenium depend on its dosage and chemical form. The narrow safety range between beneficial and toxic concentrations of selenium increases the risk of excess selenium and relevant side effects during practical application. Diverse chemical forms of selenium, including inorganic compounds, organic compounds, nanoparticles, and selenium-rich natural substances, are currently being investigated [35]. Notably, selenium nanoparticles have been found to be less toxic than inorganic and organic selenium [36]. Therefore, further research possibilities for this study include the development of a new type of Se-containing hydrogel using Se in different chemical forms to improve safety and reduce the occurrence of side effects.

5. Conclusion

In conclusion, this study provides the first evidence that a Se-containing PLGA-PEG-PLGA hydrogel provides a favorable niche for the survival and immunoregulatory activities of MSCS, ultimately improving the therapeutic efficiency of MSCs in limb ischemia. This injectable thermosensitive Se-containing hydrogel holds great promise as an MSC carrier for the treatment of limb ischemia.

Funding

This work was supported by the Major Basic Research Project of Natural Science Foundation of Shandong Province (ZR2022ZD15, ZR2020ZD15), Shandong Provincial Natural Science Foundation (ZR2023QH229, ZR2023QH243), and Natural Science Foundation of China (82270845, 82300253).

Ethics approval

The study was conducted according to the guidelines of the Declaration of Helsinki, and approved by the Ethics Committee of Qilu Hospital of Shandong University.

CRediT authorship contribution statement

Xuan Tian: Funding acquisition, Investigation, Methodology, Writing – original draft, Writing – review & editing. **Xin Yan:** Funding acquisition, Investigation, Methodology, Writing – original draft, Writing – review & editing. **Nan Zang:** Methodology, Validation, Writing – original draft. **Wu Duan:** Data curation, Methodology. **Tixiao Wang:** Data curation, Methodology, Validation, Visualization. **Xiaoxun Li:** Methodology. **Ling Ma:** Conceptualization, Methodology. **Li Chen:** Conceptualization, Funding acquisition, Supervision. **Jun Chen:** Methodology, Writing – review & editing. **Xinguo Hou:** Conceptualization, Funding acquisition, Supervision.

Declaration of competing interest

The authors declare that they have no known competing financial interests or personal relationships that could have appeared to influence the work reported in this paper.

Data availability

Data will be made available on request.

Appendix A. Supplementary data

Supplementary data to this article can be found online at https://doi.org/10.1016/j.mtbio.2024.100967.

References

[1] A. Farber, M.T. Menard, M.S. Conte, J.A. Kaufman, R.J. Powell, N.K. Choudhry, T. H. Hamza, S.F. Assmann, M.A. Creager, M.J. Cziraky, M.D. Dake, M.R. Jaff, D. Reid, F.S. Siami, G. Sopko, C.J. White, M. van Over, M.B. Strong, M.F. Villarreal, M. McKean, E. Azene, A. Azarbal, A. Barleben, D.K. Chew, L.C. Clavijo, Y. Douville, L. Findeiss, N. Garg, W. Gasper, K.A. Giles, P.P. Goodney, B.M. Hawkins, C. R. Herman, J.A. Kalish, M.C. Koopmann, I.A. Laskowski, C. Mena-Hurtado, R. Motaganahalli, V.L. Rowe, A. Schanzer, P.A. Schneider, J.J. Siracuse, M. Venermo, K. Rosenfield, B.-C. Investigators, Surgery or endovascular therapy for chronic limb-threatening ischemia, N. Engl. J. Med. 387 (2022) 2305–2316, https://doi.org/10.1056/NEJMoa2207899.

[2] M.A. Creager, K. Matsushita, S. Arya, J.A. Beckman, S. Duval, P.P. Goodney, J.A. T. Gutierrez, J.A. Kaufman, K.E. Joynt Maddox, A.W. Pollak, A.D. Pradhan, L. P. Whitsel, Reducing nontraumatic lower-extremity amputations by 20% by 2030: time to get to our feet: a policy statement from the American heart association, Circulation 143 (2021) e875–e891, https://doi.org/10.1161/CIR.0000000000000967.

[3] Y. Ding, S. Wan, L. Ma, K. Wei, K. Ye, PER1 promotes functional recovery of mice with hindlimb ischemia by inducing anti-inflammatory macrophage polarization, Biochem. Biophys. Res. Commun. 644 (2023) 62–69, https://doi.org/10.1016/j.bbrc.2023.01.001.

[4] L. Norgren, N. Weiss, S. Nikol, R.J. Hinchliffe, J.C. Lantis, M.R. Patel, H. Reinecke, R. Ofir, Y. Rosen, D. Peres, Z. Aberman, PLX-PAD cell treatment of critical limb ischaemia: rationale and design of the PACE trial, Eur. J. Vasc. Endovasc. Surg. 57 (2019) 538–545, https://doi.org/10.1016/j.ejvs.2018.11.008.

[5] A. Huang, D. Liu, X. Qi, Z. Yue, H. Cao, K. Zhang, X. Lei, Y. Wang, D. Kong, J. Gao, Z. Li, N. Liu, Y. Wang, Self-assembled GFFYK peptide hydrogel enhances the therapeutic efficacy of mesenchymal stem cells in a mouse hindlimb ischemia model, Acta Biomater. 85 (2019) 94–105, https://doi.org/10.1016/j.actbio.2018.12.015.

[6] X. Tian, H. Cao, L. Wu, W. Zheng, M. Yuan, X. Li, H. Song, Z. Shen, Heme oxygenase-1-modified bone marrow mesenchymal stem cells combined with normothermic machine perfusion repairs bile duct injury in a rat model of DCD liver transplantation via activation of peribiliary glands through the wnt pathway, Stem Cell. Int. 2021 (2021) 9935370, https://doi.org/10.1155/2021/9935370.

[7] X. Tian, L. Wu, X. Li, W. Zheng, H. Zuo, H. Song, Exosomes derived from bone marrow mesenchymal stem cells alleviate biliary ischemia reperfusion injury in fatty liver transplantation by inhibiting ferroptosis, Mol. Cell. Biochem. (2023), https://doi.org/10.1007/s11010-023-04770-8.

[8] M. Conrad, B. Proneth, Selenium: tracing another essential element of ferroptotic cell death, Cell Chem. Biol. 27 (2020) 409–419, https://doi.org/10.1016/j.chembiol.2020.03.012.

[9] Y. Yao, Z. Chen, H. Zhang, C. Chen, M. Zeng, J. Yunis, Y. Wei, Y. Wan, N. Wang, M. Zhou, C. Qiu, Q. Zeng, H.S. Ong, H. Wang, F.V. Makota, Y. Yang, Z. Yang, N. Wang, J. Deng, C. Shen, Y. Xia, L. Yuan, Z. Lian, Y. Deng, C. Guo, A. Huang, P. Zhou, H. Shi, W. Zhang, H. Yi, D. Li, M. Xia, J. Fu, N. Wu, J.B. de Haan, N. Shen, W. Zhang, Z. Liu, D. Yu, Selenium-GPX4 axis protects follicular helper T cells from ferroptosis, Nat. Immunol. 22 (2021) 1127–1139, https://doi.org/10.1038/s41590-021-00996-0.

[10] I. Alim, J.T. Caulfield, Y. Chen, V. Swarup, D.H. Geschwind, E. Ivanova, J. Seravalli, Y. Ai, L.H. Sansing, E.J. Ste Marie, R.J. Hondal, S. Mukherjee, J. W. Cave, B.T. Sagdullaev, S.S. Karuppagounder, R.R. Ratan, Selenium drives a transcriptional adaptive program to block ferroptosis and treat stroke, Cell 177 (2019), https://doi.org/10.1016/j.cell.2019.03.032, 1262-1279 e1225.

[11] Y.W. Lin, C.H. Fang, C.Y. Yang, Y.J. Liang, F.H. Lin, Investigating a curcumin-loaded PLGA-PEG-PLGA thermo-sensitive hydrogel for the prevention of alzheimer's disease, Antioxidants 11 (2022), https://doi.org/10.3390/antiox11040727.

[12] A. Limbourg, T. Korff, L.C. Napp, W. Schaper, H. Drexler, F.P. Limbourg, Evaluation of postnatal arteriogenesis and angiogenesis in a mouse model of hind-limb ischemia, Nat. Protoc. 4 (2009) 1737–1746, https://doi.org/10.1038/nprot.2009.185.

[13] F. Wu, Z. He, R. Ding, Z. Huang, Q. Jiang, H. Cui, Y. Lin, S. Huang, X. Dai, J. Zhang, Z. Wu, C. Liang, Danhong promotes angiogenesis in diabetic mice after critical limb ischemia by activation of CSE-H 2 S-vegf Axis, Evid Based Complement Alternat Med 2015 (2015) 276263, https://doi.org/10.1155/2015/276263.

[14] F. Zhang, X. Li, Y. Wei, Selenium and selenoproteins in health, Biomolecules 13 (2023), https://doi.org/10.3390/biom13050799.

[15] Y. Sun, Y. Zheng, C. Wang, Y. Liu, Glutathione depletion induces ferroptosis, autophagy, and premature cell senescence in retinal pigment epithelial cells, Cell Death Dis. 9 (2018) 753, https://doi.org/10.1038/s41419-018-0794-4.

[16] N. Cao, W. Li, B. Li, Y. Tian, D. Xu, Transcriptome profiling reveals the immune response of goose T cells under selenium stimuli, Anim. Sci. J. 88 (2017) 2001–2009, https://doi.org/10.1111/asj.12861.

[17] R. Hauffe, V. Stein, C. Chudoba, T. Flore, M. Rath, K. Ritter, M. Schell, K. Wardelmann, S. Deubel, J.F. Kopp, M. Schwarz, K. Kappert, M. Bluher, T. Schwerdtle, A.P. Kipp, A. Kleinridders, GPx3 dysregulation impacts adipose tissue insulin receptor expression and sensitivity, JCI Insight 5 (2020), https://doi.org/10.1172/jci.insight.136283.

[18] Q. Zhang, W. Liu, H.M. Zhang, G.Y. Xie, Y.R. Miao, M. Xia, A.Y. Guo, hTFtarget: a comprehensive database for regulations of human transcription factors and their targets, Dev. Reprod. Biol. 18 (2020) 120–128, https://doi.org/10.1016/j.gpb.2019.09.006.

[19] L. Qiao, X. Zhang, S. Pi, J. Chang, X. Dou, S. Yan, X. Song, Y. Chen, X. Zeng, L. Zhu, C. Xu, Dietary supplementation with biogenic selenium nanoparticles alleviate oxidative stress-induced intestinal barrier dysfunction, NPJ Sci Food 6 (2022) 30, https://doi.org/10.1038/s41538-022-00145-3.

[20] M. Wallenberg, S. Misra, M. Bjornstedt, Selenium cytotoxicity in cancer, Basic Clin. Pharmacol. Toxicol. 114 (2014) 377–386, https://doi.org/10.1111/bcpt.12207.

[21] M. Vinceti, T. Filippini, E. Jablonska, Y. Saito, L.A. Wise, Safety of selenium exposure and limitations of selenoprotein maximization: molecular and epidemiologic perspectives, Environ. Res. 211 (2022) 113092, https://doi.org/10.1016/j.envres.2022.113092.

[22] R. Ebert, M. Ulmer, S. Zeck, J. Meissner-Weigl, D. Schneider, H. Stopper, N. Schupp, M. Kassem, F. Jakob, Selenium supplementation restores the antioxidative capacity and prevents cell damage in bone marrow stromal cells in vitro, Stem Cell. 24 (2006) 1226–1235, https://doi.org/10.1634/stemcells.2005-0117.

[23] B. Gholamigeravand, S. Shahidi, S. Afshar, P. Gholipour, A. Samzadeh-Kermani, K. Amiri, M. Majidi, R. Abbasalipourkabir, M.R. Arabestani, S. Soleimani Asl, Synergistic effects of adipose-derived mesenchymal stem cells and selenium nanoparticles on streptozotocin-induced memory impairment in the rat, Life Sci. 272 (2021) 119246, https://doi.org/10.1016/j.lfs.2021.119246.

[24] J. Park, J.H. Lee, B.S. Yoon, E.K. Jun, G. Lee, I.Y. Kim, S. You, Additive effect of bFGF and selenium on expansion and paracrine action of human amniotic fluid-derived mesenchymal stem cells, Stem Cell Res. Ther. 9 (2018) 293, https://doi.org/10.1186/s13287-018-1058-z.

[25] F. Ghasemi, M. Khoshmirsafa, E. Safari, M. Asgari, M. Alemrajabi, S. Nojehdehi, S. Khorrami, Vitamin E and selenium improve mesenchymal stem cell conditioned media immunomodulatory effects, Stem Cell Invest. 8 (2021) 9, https://doi.org/10.21037/sci-2020-008.

[26] B. Rahimi, M. Panahi, H. Lotfi, M. Khalili, A. Salehi, N. Saraygord-Afshari, E. Alizadeh, Sodium selenite preserves rBM-MSCs' stemness, differentiation potential, and immunophenotype and protects them against oxidative stress via activation of the Nrf2 signaling pathway, BMC Complement Med Ther 23 (2023) 131, https://doi.org/10.1186/s12906-023-03952-7.

[27] Z. Yin, C. Qin, S. Pan, C. Shi, G. Wu, Y. Feng, J. Zhang, Z. Yu, B. Liang, J. Gui, Injectable hyperbranched PEG crosslinked hyaluronan hydrogel microparticles containing mir-99a-3p modified subcutaneous ADSCs-derived exosomes was beneficial for long-term treatment of osteoarthritis, Mater Today Bio 23 (2023) 100813, https://doi.org/10.1016/j.mtbio.2023.100813.

[28] H. Zhang, M. Zhang, X. Zhang, Y. Gao, Y. Ma, H. Chen, J. Wan, C. Li, F. Wang, X. Sun, Enhanced postoperative cancer therapy by iron-based hydrogels, Biomater. Res. 26 (2022) 19, https://doi.org/10.1186/s40824-022-00268-4.

[29] C.K. Lee, D.F. Atibalentja, L.E. Yao, J. Park, S. Kuruvilla, D.W. Felsher, Anti-PD-L1 F(ab) conjugated PEG-PLGA nanoparticle enhances immune checkpoint therapy, Nanotheranostics 6 (2022) 243–255, https://doi.org/10.7150/ntno.65544.

[30] Y.G. Yuan, J.L. Wang, Y.X. Zhang, L. Li, A. Reza, S. Gurunathan, Biogenesis, composition and potential therapeutic applications of mesenchymal stem cells derived exosomes in various diseases, Int. J. Nanomed. 18 (2023) 3177–3210, https://doi.org/10.2147/ijn.S407029.

[31] C.T. Huerta, F.A. Voza, Y.Y. Ortiz, Z.J. Liu, O.C. Velazquez, Mesenchymal stem cell-based therapy for non-healing wounds due to chronic limb-threatening ischemia: a review of preclinical and clinical studies, Front Cardiovasc Med 10 (2023) 1113982, https://doi.org/10.3389/fcvm.2023.1113982.

[32] Y. Wang, J. Fang, B. Liu, C. Shao, Y. Shi, Reciprocal regulation of mesenchymal stem cells and immune responses, Cell Stem Cell 29 (2022) 1515–1530, https://doi.org/10.1016/j.stem.2022.10.001.

[33] S. Schrepfer, T. Deuse, H. Reichenspurner, M.P. Fischbein, R.C. Robbins, M. P. Pelletier, Stem cell transplantation: the lung barrier, Transplant. Proc. 39 (2007) 573–576, https://doi.org/10.1016/j.transproceed.2006.12.019.

[34] M.P. Rayman, Selenium intake, status, and health: a complex relationship, Hormones (Basel) 19 (2020) 9–14, https://doi.org/10.1007/s42000-019-00125-5.

[35] M. Kielczykowska, J. Kocot, M. Pazdzior, I. Musik, Selenium - a fascinating antioxidant of protective properties, Adv. Clin. Exp. Med. 27 (2018) 245–255, https://doi.org/10.17219/acem/67222.

[36] C. Ferro, H.F. Florindo, H.A. Santos, Selenium nanoparticles for biomedical applications: from development and characterization to therapeutics, Adv. Healthcare Mater. 10 (2021) e2100598, https://doi.org/10.1002/adhm.202100598.